Electropolymerizable 2,2′-Carboranyldithiophenes. Structure−Property Investigations of the Corresponding Conducting Polymer Films by Electrochemistry, UV−Visible Spectroscopy and Conducting Probe Atomic Force Microscopy

Frédéric Barrière,[†] Bruno Fabre,*[,†] Erhong Hao,[‡] Zorabel M. LeJeune,[‡] Euiyong Hwang,[‡] Jayne C. Garno,[‡] Evgueni E. Nesterov,[‡] and M. Graça H. Vicente[‡]

CNRS UMR 6226, Sciences Chimiques de Rennes, Matière Condensée et Systèmes Electroactifs (MaCSE), Université de Rennes 1, Campus de Beaulieu, 35042 Rennes Cedex, France, and Department of Chemistry, Louisiana State University, Baton Rouge, Louisiana 70803

Received October 22, 2008; Revised Manuscript Received February 27, 2009

ABSTRACT: Carborane-functionalized conducting polymer films have been electrogenerated in dichloromethane from the anodic oxidation of *ortho*- (**1**), *meta*- (**3**) and *para*-carborane (**4**) isomers linked to two 2-thienyl units. The corresponding electrochemical response was characterized by a broad reversible redox system corresponding to the p-doping/undoping of the polythiophene backbone, the formal potential of which increased in the order poly(**1**) < poly(**3**) < poly(**4**), from ca. 0.50 to 1.15 V vs Ag/Ag^+ 10^{-2} M. From further UV−visible spectroscopy analysis, the optical band gap was estimated at 1.8, 2.0 and 2.2 eV for poly(**1**), poly(**3**) and poly(**4**), respectively. The more conjugated and electroconductive character of poly(**1**) is ascribed to a more planar conformation of the conjugated backbone resulting from an intramolecular $\beta-\beta'$ cyclization reaction in the monomer, consequently yielding a fused conjugated polymer. Molecular modeling calculations using the DFT method support this hypothesis. The surface topography and maps of the conductive domains of the electropolymerized films were evaluated by conducting probe AFM. The three polymers exhibit fairly similar morphological characteristics and a surface roughness of ∼2 nm. Current−voltage ($I-V$) characteristics of conducting AFM tip-carborane polymer−ITO junctions showed that poly(**1**) had the highest conductivity.

1. Introduction

Heterocyclic conjugated polymers such as polypyrrole and polythiophene have important applications as conducting electroactive materials, in microelectronics, electrochemical switching, photovoltaics, organic light-emitting diodes, organic field-effect transistors, energy storage and conversion, electrochromic and electromechanical devices, and in chemical and physical sensing.[1−8] Since their discovery in the mid-1970s, conducting polymers have been an active area of research for both academic and industrial investigators. One advantage of using conjugated polymers is the ability to tune the polymer properties at the molecular level, typically accomplished through synthetic modification of the monomer precursors, or by alteration of the electronic structure of the polymer backbone via varying the nature of the dopant, the doping level, and by blending with other polymers. In addition, polymeric materials are light in weight, easily processed, and flexible.

The major obstacles to practical applications of conductive polymers are (1) the relatively poor environmental stability (mainly due to their rapid oxidation by oxygen and Joule heating) and (2) their short lifetime when electrochemically cycled between oxidation states. Thus the development of new high-performance conducting polymers with high chemical, electrochemical and thermal stability remains a challenge. Various methodologies have been proposed to overcome these problems, including the use of new electrolytes (e.g., ionic liquids),[8] nanoparticles,[9,10] and the preparation of new high-performance conductive polymers by designing new monomers and/or controlling the effective π-conjugation of the polymer backbone.[11−13]

Toward the goal of designing optimal conducting materials of high environmental stability for various applications, the functionalization of conjugated polymers with organoborane groups is particularly attractive since boron-containing polymers have been historically commercialized primarily because of their remarkable chemical and thermomechanical resistance (e.g., Olin's DEXSIL and Union Carbide's UCARSIL) and have found applications as sensor, optical and separation materials.[14,15] Among the organoboranes, carboranes are ideal candidates for chemical and thermal strengthening of organic polymers. Carboranes, in both neutral and anionic forms, are boron clusters with delocalized electrons and unique properties, including high hydrophobic character, low nucleophilicity, electron-withdrawing nature and exceptional chemical, thermal and optical stability as a result of their three-dimensional aromatic character.[16,17] Furthermore, the anionic open cage carborane derivatives form strong sandwich-type complexes with a variety of metal ions (e.g., Co, Ni, Fe).[18,19] Therefore incorporation within organic materials is a practical approach to confer novel properties upon the host matrix, such as high thermal and chemical stability, unique optoelectronic characteristics and an ordered structure. Several polymers have been synthesized and characterized containing carborane groups, usually linked to the host molecule by aromatic spacers.[20−25] These macromolecular systems showed extreme resistance to combustion and a two-dimensional grid-shaped structure using the boron cage as a molecular connector. However, such materials were usually synthesized in several steps and did not show peculiar electronically conducting properties which preclude them from some applications, such as electrochromic and charge storage devices. Some years ago, Teixidor's group[26−29] and ourselves[30−33] have prepared novel electroconducting polypyrroles and polythiophenes functionalized with various neutral and anionic carboranes. These materials, which were

* Corresponding author. E-mail: fabre@univ-rennes1.fr.
[†] CNRS UMR 6226, Sciences Chimiques de Rennes, Matière Condensée et Systèmes Electroactifs (MaCSE), Université de Rennes 1.
[‡] Department of Chemistry, Louisiana State University.

10.1021/ma802369z CCC: $40.75
Published on Web 03/24/2009

Scheme 1. Synthesis of Carboranes Linked to 2-Thienyl Units[a]

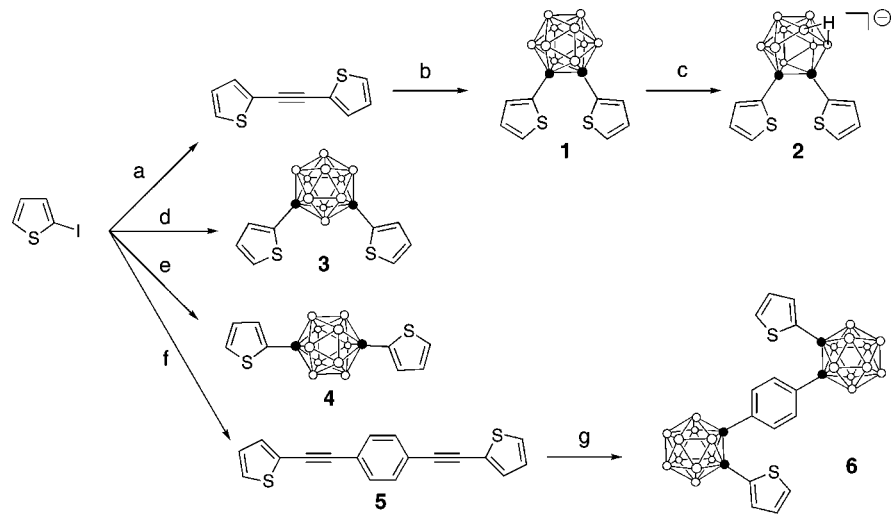

[a] Reaction conditions: (a) $Pd(PPh_3)_2Cl_2$, CuI, DBU, H_2O, ethynyltrimethylsilane; (b) $B_{10}H_{14}$, diethyl sulfide, toluene; (c) THF/1.0 M Bu_4NF; (d) *m*-$Li_2C_2B_{10}H_{10}$, CuI, 1,2-dimethoxyethane, pyridine; (e) *p*-$Li_2C_2B_{10}H_{10}$, CuI, 1,2-dimethoxyethane, pyridine; (f) $Pd(PPh_3)_2Cl_2$, CuI, diethylamine, 1,4-diethynylbenzene; (g) $B_{10}H_{14}$, diethyl sulfide, toluene.

electrochemically generated in one step, exhibited a strong enhancement of their electrochemical stability and overoxidation resistance compared with unsubstituted parent conducting polymers.

Concerning the development of carborane-functionalized conducting polymers, we present herein the detailed investigation of a series of electropolymerizable carborane-substituted di(2-thienyl) units (Scheme 1). By introducing thiophene rings on the *ortho*-, *meta*- and *para*-positions of the carborane, we aim to fully analyze the effects of the position and the charge of the boron cluster on the electropolymerization efficiency and the properties of the resulting conducting polymer films. Furthermore, UV−visible spectroscopy and conducting AFM techniques provide insight on the effective π-conjugation length as well as on the morphological characteristics and the local charge transport properties of the polymers. Density functional theory (DFT) calculations have been used to obtain information about the structure of the possible reactive intermediates which were electrogenerated from the monomers and to help in the interpretation of the experimental (optical and electrochemical) data.

2. Experimental Section

General Data. Commercially available solvents and starting materials were used without further purification. All reactions were monitored by thin layer chromatography (TLC) using 0.25 mm silica gel plates with or without UV indicator (60F-254). Silica gel Sorbent Technologies 32−63 μm was used for flash column chromatography. A solution of 1 g of $PdCl_2$ in 80 mL of water and 20 mL of 36% HCl solution was used to detect carborane-containing molecules upon heating the TLC plates. ^{1}H- and ^{13}C NMR were obtained on a DPX-250 or an ARX-300 Bruker spectrometer; chemical shifts (δ) are given in ppm relative to $CDCl_3$ (7.26 ppm, ^{1}H) or acetone-d_6 (2.05 ppm, ^{1}H; 206 ppm, ^{13}C). MALDI−TOF mass spectra were obtained on an Applied Biosystems QSTAR XL.

Di(2-thienyl)carboranes **1**, **3** and **4**, bearing respectively an *ortho*-, *meta*- or *para*-carborane group, were prepared from 2-iodothiophene in 24%, 36%, and 39% overall yield respectively, as reported in our previous communication.[31] The anionic *nido*-carboranylthiophene **2** was obtained in high yield by fluoride-induced deboronation of the *closo*-carborane cages using tetrabutylammonium fluoride.

Synthesis of the Anionic *nido*-Carboranylthiophene 2. Compound **1** (310 mg, 1.0 mmol) was dissolved in 20 mL THF and 3.0 mL *n*-Bu_4NF solution (1.0 M in THF) was added. The reaction mixture was stirred at 60 °C for 30 min until all the starting material was consumed and then was poured into 50 mL water and extracted with ethyl acetate (3 × 50 mL). The organic layer was dried over Na_2SO_4 and concentrated. The residue was passed through a pad of silica gel, using ethyl acetate as the eluent. The target compound was obtained in 95% yield as a white powder. ^{1}H NMR (acetone-d_6, 400 MHz) 6.83−6.85 (2H, m), 6.52−6.57 (4H, m), 1.50−3.50 (9H, br), −2.00 to −2.50 (1H, br); ^{13}C NMR (acetone-d_6, 100 MHz) 147.5, 127.2, 125.4, 123.6, 76.0, 58.8, 23.9, 19.8, 13.4. HRMS (ESI): calcd $[M - NBu_4]^-$, $C_{10}H_{16}B_9S_2$, 297.1504; found, 297.1562.

Synthesis of Di(2-thienyl) *p*-Dicarboranylbenzene 6. Compound **5** was prepared in 71% yield as a yellow powder using Sonogashira coupling according to a literature procedure.[34] A mixture of decaborane (2.44 g, 3.0 mmol) and diethyl sulfide (9.0 mL, 37 mmol) in 20 mL of dry toluene was heated at 40 °C for 2 h under argon, and then the temperature was raised to 60 °C for 3 h. Then **5** (1.45 g, 5 mmol) in 20 mL of toluene was added into the mixture by syringe, and the mixture was heated at 80 °C for 2 days under argon. After complete disappearance of **5** monitored by TLC, the mixture was cooled to room temperature and the excess of decaborane was destroyed by adding methanol. The solvent was removed under reduced pressure and ethanol was added to remove diethyl sulfide via codistillation. The residue was purified by column chromatography on silica gel using 10% dichloromethane in hexane, giving the title compound as a light yellow powder (0.789 g) in 31% yield. ^{1}H NMR (250 MHz, $CDCl_3$) δ 7.33−7.34 (4H, m), 7.06−7.11 (2H, m), 6.97−6.99 (2H, m), 6.70−6.73 (2H, m), 1.5−3.5 (20H, br); MALDI−TOF $[M]^+$: found, 526.82; calcd for $C_{18}H_{30}B_{20}S_2$, 526.78.

Electrochemical Characterizations. Tetra-*n*-butylammonium hexafluorophosphate Bu_4NPF_6 was purchased from Fluka (puriss, electrochemical grade). Anhydrous methylene chloride CH_2Cl_2 (less than 50 ppm water from Merck) was used as received. The electrolytic medium was dried *in situ* over activated, neutral alumina from Aldrich. Alumina was previously activated at 450 °C under vacuum for several hours. Linear potential sweep cyclic voltammetry experiments were performed with an Autolab PGSTAT 20 potentiostat from Eco Chemie B.V., equipped with General Purpose Electrochemical System GPES software (version 4.5 for Windows). The working electrode was a 1 mm-diameter platinum disk (area: 0.8 mm^2) and the counter electrode was a glassy carbon rod. Potentials were relative to the system 10^{-2} M Ag^+|Ag in acetonitrile and the ferrocene/ferrocenium couple in CH_2Cl_2 + 0.2 M Bu_4NPF_6 was observed at $E^{\circ\prime} = 0.19$ V vs this reference. Solution resistance

was compensated by positive feedback. Electrochemical measurements were carried out at room temperature (20 ± 2 °C) and under a constant flow of argon.

UV−Visible Spectroelectrochemistry. UV−visible absorption spectra were recorded on a Shimadzu Multispec-1501 spectrophotometer (190−1100 nm scan range) interfaced with a microcomputer for data acquisition and quartz SUPRASIL cells from Hellma (1 cm path length) were used. The polymer films were grown on an indium tin oxide (ITO) coated glass slide electrode.

Conducting Atomic Force Microscopy (AFM). *(a). Sample Preparation.* Indium tin oxide (ITO) coated glass slides (8−12 Ω cm^{-2} surface resistivity, from Delta Technologies, Ltd.) were ultrasonicated in CH_2Cl_2 for 20 min, followed by rinsing with acetone and deionized water. The precleaned slides were subjected to an RCA-type cleaning procedure by keeping in a water−30% H_2O_2−30% aqueous NH_3 (5:1:1) mixture at 70 °C for 1 h. The substrates were then rinsed with copious amount of deionized water and dried in N_2 flow at room temperature for 2 h. The carborane-based polymer films for microscopy studies were prepared by potentiodynamical electrodeposition (20 scans; 0.1 V/s) using the ITO/glass substrate as a working electrode (approximative area 1.1 × 2.5 cm^2), Ag/Ag^+ reference electrode, and Pt gauze counter electrode. The monomer concentration was 5 mM in CH_2Cl_2 + 0.1 M Bu_4NPF_6. The potentials were scanned in the range of 0−1.7 V for monomers **3** and **4**, and 0−1.2 V for monomer **1**. After polymerization was complete, each sample was rinsed with copious amount of CH_2Cl_2 and dried in N_2 flow. The substrate was placed in a monomer-free electrolyte for CV characterization that included 10 successive scans at the scanning rate of 0.1 V/s. At the end of the last scan, the sample was left at the standby potential of −1.0 V to ensure leaving the polymer in an electrochemically undoped state. Finally, the sample was washed with copious amount of CH_2Cl_2 and dried in N_2 flow.

(b). Microscopy. Images of the electropolymerized films were acquired in ambient conditions with a model 5500 scanning probe microscope (SPM) equipped with Picoscan v5.3.3 software (Agilent Technologies, Inc., Chandler, AZ). The nosecone of the scanner contained a preamp module with 1 nA/V sensitivity for current-sensing atomic force microscopy (CS-AFM). Conductive tips with an average force constant of 6 N/m were used for both current and topography imaging (MikroMasch CSC11/Ti−Pt, San Jose, CA). The tip coating consisted of a 10 nm layer of Pt on a sublayer of 20 nm Ti, which was coated on both the tip and reflective side of the cantilever. The resulting radius of the tip with the coating was ∼40.0 nm. Topographic and current images were acquired simultaneously with a bias voltage of −0.1 V applied to the samples. A scan rate of 3.0 nm/s for 512 lines/frame was used for current imaging. The set point was chosen at a minimum value to prevent damage to the film and the cantilever. Estimates of surface coverage were obtained with the UTHSCA Image Tool.[59] The CS-AFM images were converted to grayscale bitmaps, and a threshold value was selected visually for conversion to black and white pixels. The percentage of colored pixels provided a relative estimate of surface coverage.

Computational Studies. Full geometry optimization with DFT[35,36] calculations were performed with the hybrid Becke-3 parameter exchange functional[37−39] and the Lee−Yang−Parr nonlocal correlation functional[40] (B3LYP) implemented in the Gaussian 03 (Revision D.02) program suite[41] using the 6-31G* basis set[42] and the default convergence criterion implemented in the program. The figures were generated with MOLEKEL 4.0.[43]

3. Results and Discussion

3.1. Electrochemistry of the Monomers and Their Corresponding Polymer Films. The cyclic voltammetry characterization of the neutral di(2-thienyl) carboranes **1**, **3**, and **4** at 10^{-2} M in thoroughly dried CH_2Cl_2 + 2 × 10^{-1} M Bu_4NPF_6 revealed three irreversible oxidation peaks when cycled between 0.0 and 2.4 V vs Ag/Ag^+ 10^{-2} M (Table 1). The oxidation potentials of each system were found to increase in the order **1** < **3** < **4**. Since unsubstituted carboranes are not oxidized under these electrolytic conditions, these can be assigned to the oxidation of the 2-thienyl rings into reactive radical cation species. It must be noticed that the three carboranes were not reduced down to −2.5 V. For the Z-shaped compound **6**, a single irreversible anodic peak was observed at a relatively high potential, ca. 2.2 V while the cathodic scan showed two quasi-reversible systems at −1.40 and −1.71 V (average of anodic and cathodic peak potentials) corresponding to the formation of the radical anion and dianion forms respectively.[44] Thus, the electrochemical behavior of **6** is consistent with the stronger electron-withdrawing character of the *p*-dicarboranylbenzene core between the two 2-thienyl units. Cyclic voltammogram of the carborane **2** which is the anionic analogue of **1** was characterized by two irreversible anodic peaks at 0.75 and 0.98 V followed by a broad ill-defined shoulder at 1.42 V. Similarly to the other di(2-thienyl) carboranes, this compound was not electrochemically reduced down to −2.5 V. The first system can be attributed to the oxidation of the anionic *nido*-carborane cage, which is consistent with other electrochemical data reported for *nido*-carborane-substituted pyrroles[30,32] and thiophenes.[30]

Table 1. Cyclic Voltammetry Data of 2,2′-Carboranyldithiophenes at 10^{-2} M in CH_2Cl_2 + 2 × 10^{-1} M Bu_4NPF_6[g]

	monomer		polymer	
	E_{ox}/V[a]	E_{red}/V[b]	$E^{\circ\prime}{}_p$/V[c]	$E_{pc\ n}$/V[d]
1	0.90; 1.70; 2.15	*e*	0.53	−1.96
2	0.75; 0.98; 1.42	*e*	*f*	*f*
3	1.11; 1.84; 2.18	*e*	0.88	−1.82
4	1.12; 1.82; 2.06	*e*	1.16	−2.37
6	2.20	−1.40; −1.71	*f*	*f*

[a] Irreversible anodic peak potentials corresponding to the monomer oxidation. [b] Formal potential corresponding to the quasi-reversible reduction steps. [c] Formal potential corresponding to the reversible p-doping/undoping of the electrogenerated polymer (average of anodic and cathodic peak potentials). [d] Cathodic peak potential corresponding to the n-doping of the electrogenerated polymer. [e] No reduction wave was observed. [f] No conducting polymer film was electrogenerated. [g] Potential scan rate: 0.1 V s^{-1}. All potentials are reported vs. Ag/Ag^+ 10^{-2}M.

Among all these carboranes, only the electrochemical oxidation of **1**, **3** and **4** led to the formation of conducting polymer deposits on the electrode surface. Such films could be electrogenerated either potentiodynamically or potentiostatically with no significant effect of the electropolymerization method on their respective electrochemical responses. Representative cyclic voltammograms corresponding to the potentiodynamical electropolymerization of these compounds are shown in Figure 1. As can be seen, electropolymerization of **3** and **4** occurred at a higher oxidation potential than that required for the electropolymerization of **1**. In contrast to the facile electropolymerization of **1**, **2** did not yield a conducting polymer deposit under a variety of experimental conditions, for example using different monomer concentrations, oxidation potentials, solvents and methods. Instead, a poorly electroactive film was electrogenerated yielding the progressive passivation of the electrode surface (Figure 1B). Oxidation of the carborane anion prior to the aromatic ring is believed to lower the reactivity of the thiophene radical cation intermediates and/or to promote the coupling of the oxidized thiophene rings on the defect sites. For **6**, the strong electron-withdrawing character of the bridge between the two thienyl units impeded the electropolymerization reaction to occur.

Further information on the deposition mechanism of poly(**1**), poly(**3**), and poly(**4**) was provided from the chronoamperometric plots monitored during the potentiostatic electrodeposition experiments. The current *I* versus time *t* profiles (not shown) of the three monomers oxidized at their respective optimal

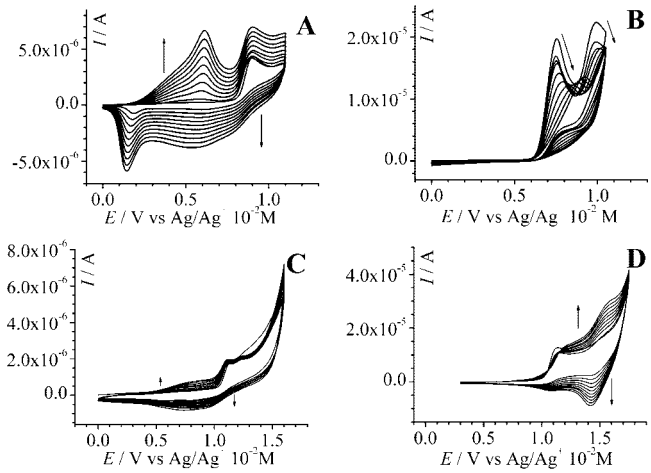

Figure 1. Successive cyclic voltammograms of **1** (A), **2** (B), **3** (C), and **4** (D) at 10^{-2} M in $CH_2Cl_2 + 2 \times 10^{-1}$ M Bu_4NPF_6 (0.1 V s^{-1}).

electropolymerization potential were characterized by an initial decrease of the current with time over the first 20−40 s following a $I - t^{-1/2}$ relationship as expected for a diffusion-controlled process. After this transient period, the current monitored for **1** was found to increase linearly with time whatever the applied electropolymerization potential. Such a time dependency is consistent with a progressive nucleation and 3D growth mechanism.[45,46] For the electrodeposition of unsubstituted polythiophene, a linear current vs t^2 relationship was observed and such a behavior was ascribed to an instantaneous nucleation/3D growth mechanism.[47,48] In the case of **2** and **3**, the current was approximately constant with time which suggests that the growth rate of these polymers was much slower than that of poly(**1**).

Following their electrosynthesis, the polymer films were examined in a monomer-free electrolytic medium. Their electrochemical response was characterized by a broad reversible redox system corresponding to the p-doping/undoping of the polythiophene backbone, the formal potential of which increased in the order poly(**1**) (0.53 V) < poly(**3**) (0.88 V) < poly(**4**) (1.16 V) as observed for the monomers (Table 1 and Figure 2). Additionally, a cation doping was also visible at potentials close to −2.0 V but, in contrast to the p-doping, the n-doped form of these polymers was poorly stable and extremely sensitive to traces of water or oxygen.

3.2. UV−Visible Spectroscopy Analysis of Polymers. To gain further insight into the electronic properties of carborane-functionalized polythiophenes, a UV−visible spectroscopy analysis was performed focusing on the electroactive polymers electrogenerated from **1**, **3**, and **4**. In their neutral form, the three polymers poly(**1**), poly(**3**), and poly(**4**) displayed similar absorptions, with a bathochromic shift decreasing in the order poly(**1**) > poly(**3**) > poly(**4**). The absorption maximum for the interband $\pi \rightarrow \pi^*$ transition was observed at 488 nm (2.5 eV) and 425 nm (2.9 eV) for poly(**3**) and poly(**4**), respectively (Figure 3). In contrast, the neutral poly(**1**) showed a well-defined vibronic fine structure with maxima at 528 (2.3 eV), 565 (2.2 eV), and 615 nm (2.0 eV). Such optical features which are not observed for poly(**3**) and poly(**4**) have often been reported for highly conjugated, ordered polymers.[49] The onset of the absorption band was used to determine the optical band gap of these polymers. Values of 1.8, 2.0, and 2.2 eV were obtained for poly(**1**), poly(**3**), and poly(**4**) which are consistent with the electrochemical band gaps determined from the potential differences between the onset of the p- and n-doping redox waves, namely 1.85, 1.92, and 2.35 eV for poly(**1**), poly(**3**), and poly(**4**), respectively (Figure 2). Furthermore, the band gap calculated for poly(**4**) was similar to that reported for poly(di-2-thienyl-*p*-phenylene)[50] which indicates that the electronic and steric effects of the carboranyl moiety on the mean conjugation length of the resulting polymer are not very different from those of a benzene ring. A similar bathochromic shift was also observed for the oxidatively doped, as-grown polymers that displayed a new doping-induced band at 810, 730, and 686 nm for poly(**1**), poly(**3**) and poly(**4**) respectively. Based on the ratio between the absorbance maxima of the $\pi \rightarrow \pi^*$ transition band and the doping band, it can be concluded that the charge carriers in the films of doped poly(**3**) and poly(**4**) are a combination of polaron and bipolaron states while poly(**1**) contains rather high density of bipolarons.

From the electrochemical and optical data, it can be concluded that poly(**1**) is more conjugated and more electroconducting than the other two related polymers. Such observations could be explained by a more planar conformation of the conjugated backbone resulting from an intramolecular $\beta-\beta'$ cyclization reaction in the monomer and consequently yielding a fused conjugated polymer. Hence, electrolysis experiments aiming at isolating the intramolecular cyclization product have been performed at different oxidation potentials ranging from 0.7 to 0.9 V vs Ag/Ag^+ 10^{-2} M (i.e., before and in the rising part of the oxidation peak of **1**). No oxidation product was electrogenerated at 0.7 V whereas the oxidation of **1** at 0.8 or 0.9 V yielded a polymer film deposited onto the electrode surface, and no electroactive material was detected in solution. As a matter of fact, the oxidation of **1** is expected to generate the intramolecular cyclization product in its oxidized form owing to the extension of the conjugated system. As already demonstrated for the electropolymerization of other thiophene derivatives,[2] this reaction intermediate is expected to be highly reactive and undergo a further fast coupling reaction to give a longer chain oligomer. As a consequence, this prevents the isolation of such a product in solution. Molecular modeling calculations using the DFT method have therefore been performed to test the hypothesis of intramolecular $\beta-\beta'$ cyclization (*vide infra*).

3.3. Molecular Modeling Studies. The calculated absolute energy after gas phase geometry optimization of di(2-thienyl)-carboranes **1**, **3** and **4** at the B3LYP/6-31G* level of theory showed that the *meta*- and *para*- isomers were respectively 0.59 and 0.71 eV more stable than the *ortho*-isomer. This trend might be expected on the basis of the sterically less hindered thiophene groups in *meta*- and *para*-isomers as compared to the *ortho*-isomer. Interestingly, within each isomer, the *syn* and *anti* rotamers having the thiophene sulfur atoms pointing respectively both up or up/down had nearly the same energy, for example the *syn*- and *anti-ortho* isomers absolute energies only differed by ca. 0.01 eV. This is consistent with the published crystal structures of **1**, **3** and **4** where disorder in the thiophene ring has been reported, as is common for this type of molecule.[31] The calculated energy level of the HOMO indicated that **1** (−6.77 eV) should in principle be harder to oxidize with respect to **3** (−6.52 eV) and **4** (−6.32 eV). This is the reversed order of what was observed experimentally for the anodic peak potential of the first oxidation of **1** (0.9 V), **3** (1.11 V), and **4** (1.12 V). However, one should keep in mind that the first anodic electron transfers in **1**, **3**, and **4** are irreversible so that it is not straightforward to relate its value to the HOMO level, since their formal oxidation potential certainly depends on both the nature and rate of the chemical reaction following electron transfer. Instead, the fact that the onset oxidation potential of **1** was lower than that of **3** and **4** and, in addition, opposite to the expected trend considering the calculated energy level of the HOMO suggests that the driving force of the following reaction (polymerization) is higher for **1** rather than in the case of **3** and

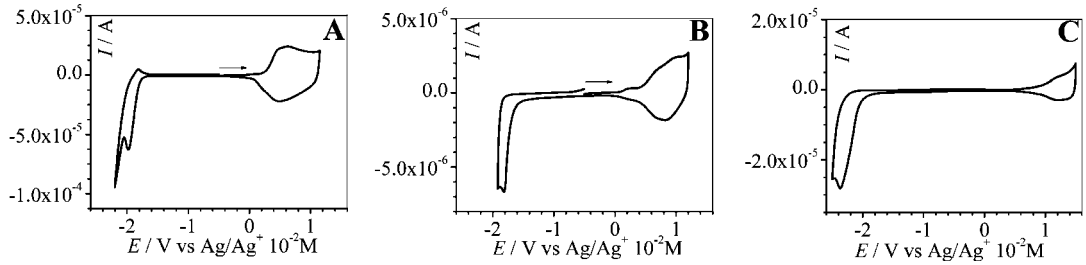

Figure 2. Electrochemical responses of the electrogenerated poly(**1**) (A), poly(**3**) (B), and poly(**4**) (C) films in CH_2Cl_2 + 2 × 10^{-1} M Bu_4NPF_6 at 0.1 V s^{-1}.

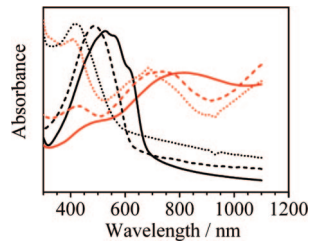

Figure 3. UV−vis spectra of oxidatively doped, as-grown (red) and electrochemically undoped (black) poly(**1**) (solid), poly(**3**) (dashed), and poly(**4**) (dotted) films.

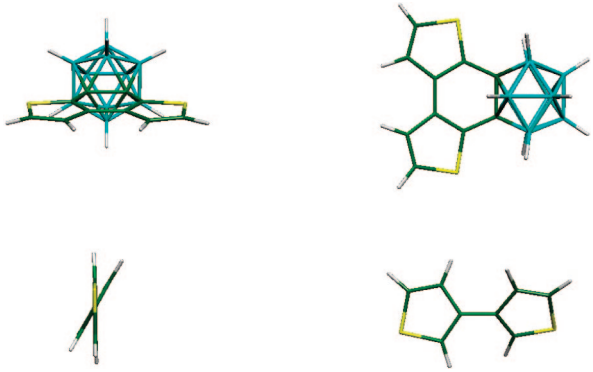

Figure 4. Comparison of **1** after intramolecular $\beta-\beta'$ cyclization (planar dithienyl, top) with dithienyl (30.2° dihedral angle, bottom) using Gaussian03 B3LYP/6-31G* calculations.

4. A cursory look at the structures of these three isomers immediately suggests an intramolecular coupling mechanism that should be possible for **1** but unreasonable for **3** and **4** (the distance between the two thienyl carbon atoms linked to the carborane moiety are respectively *ca.* 3.2, 5.2 and 6.1 Å). Indeed, calculation of the *ortho* isomer after intramolecular cyclization yielded a stable structure having a planar dithiophene ring anchored to the carborane moiety (Figure 4). Comparison with dithiophene itself shows that this molecule is not planar with a dihedral angle of 30.2° between the two constitutive thiophene rings. This has important consequences for the structure and properties of the resulting electropolymerized film in terms of higher conjugation length and related conducting properties. This result is consistent with the reported electrochemical and optical properties of the **1**-based polymer with respect to the **3**- and **4**-based polymers. The key intramolecular reaction that is not possible for **3** and **4** may also explain why **1** underwent an unexpectedly facile electrochemical oxidation.

3.4. Conducting Probe AFM Characterization of the Polymers. Current imaging is becoming a common scanning probe microscopy (SPM) characterization for thin films and nanomaterials.[51−54] Current images can be simultaneously acquired with topography by applying a bias voltage to a conductive or semiconductive sample, and measuring the current with a conductive probe, when the tip is placed in contact with the sample surface. More specifically for our study, CS-AFM was used both to characterize the surface topography and map the conductive domains of the electropolymerized films. The doped as-grown poly(**1**), poly(**3**) and poly(**4**) films were analyzed after anodic electrodeposition on indium−tin-oxide (ITO) substrates. The AFM images of the bare ITO surface were consistent with previous reports of the morphology of sputter-deposited ITO/glass (Figure 5A).[55,56] The angular terraces and clefts of the irregular surface domains are visible. The flat areas of the terraces ranged from 150 to 900 nm in lateral dimension. With a close-up view (1 × 1 μm^2), the grain nanostructures of the polycrystalline ITO were revealed as smooth and round, of relatively monodisperse dimensions ranging from 20−70 nm.

A side-by-side comparison of the topography images reveals a regular globular morphology for the polymer films (Figure 5B−D). The topography views evidence globular structures with randomly distributed protrusions of various dimensions ranging from 2 to 10 nm in height. The angular terraces of the ITO substrate are still discernible in the topography images. The data for the polymer samples was acquired using the same AFM probe, so that the observed morphology differences do not necessarily result from changes in tip dimensions. The overall root-mean-square (rms) roughness measured 2.4, 2.1, and 2.7 nm for poly(**1**), poly(**3**), and poly(**4**), respectively. The size of the globular structures are nearly identical for the poly(**1**) and poly(**3**) samples (Figure 5B,C), however the round structures are slightly larger for poly(**4**) (Figure 5D) following a trend similar to the roughness measurements.

The concurrently acquired conductivity frames obtained at an applied bias of −0.1 V furnish a nanoscale map of differences in current conduction for each sample (Figure 5I−L). At the nanoscale, the overall surface exhibits relatively nonuniform electronic conductivity. The round areas of the protrusions conducted current poorly. The bright areas at the edges were more conductive, the magnitude of the current ranged between 0.1 and 0.3 nA. The current images exhibit relatively uniform electronic conductivity within the globular domains at the nanoscale, however the peripheral areas at the edges show higher conductivity. The current magnitude varied according to nanoscale surface features and the more conductive regions indicated by the brighter areas covered 42%, 35%, 18%, and 36% of the surface for ITO, poly(**1**), poly(**3**), and poly(**4**), respectively (Figures 5I−5L). The surface topography of the underlying ITO substrate also influenced the measurement of current passing between the tip and sample. Basically, current images are a function of the tip profile and a changing surface geometry which is affected by the contact area between the tip and surface.

From this comparative study, it could be concluded that the morphology of the three electropolymerized films displayed fairly similar characteristics at the nanoscale, with comparable surface roughness of ∼2 nm. The angular terraces and small irregular domains of the underlying ITO substrate predominated in the resulting surface topography. Comparing the maps of

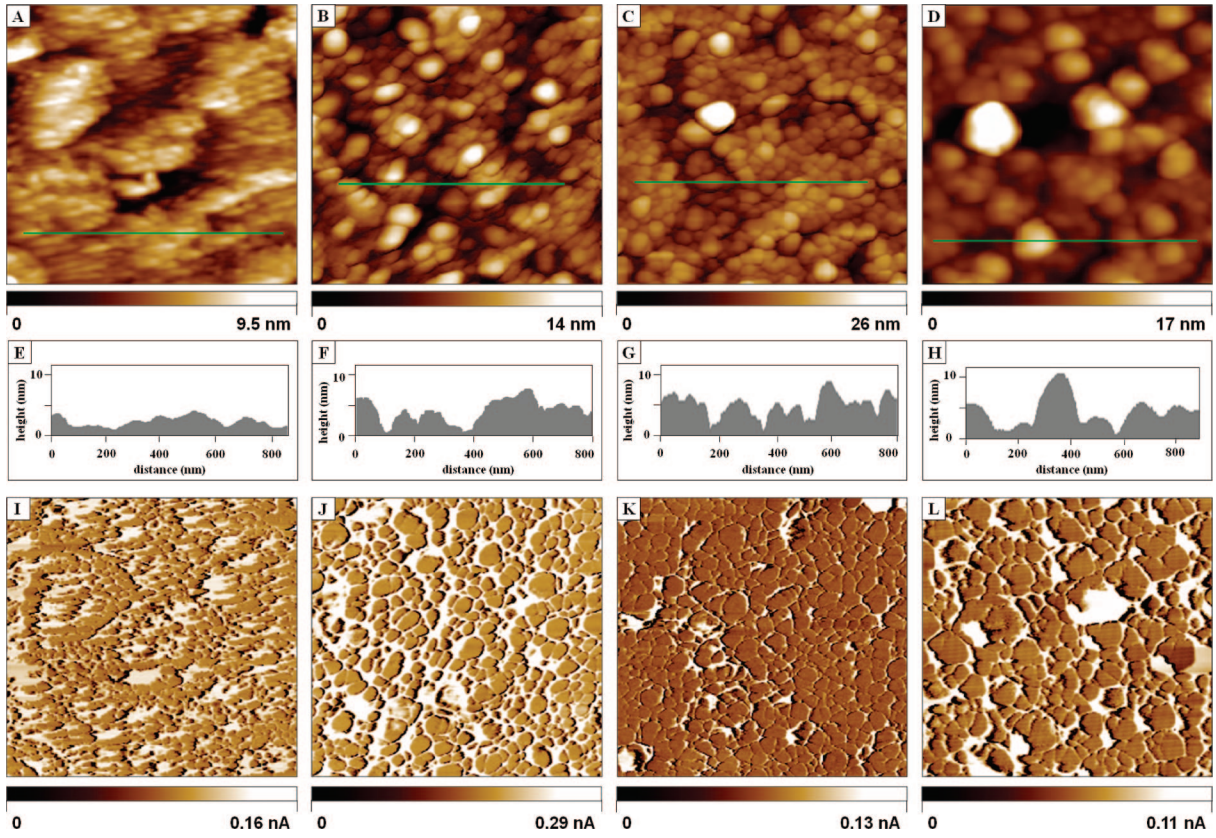

Figure 5. Surface morphology and current maps of bare ITO and coated with carborane-functionalized polymer films. AFM images and corresponding cross-section profiles for ITO (A, E), poly(**1**) (B, F), poly(**3**) (C, G), and poly(**4**) (D, H). Simultaneously generated current images taken at −0.1 V of ITO (I), poly(**1**) (J), poly(**3**) (K), and poly(**4**) (L). The scan size for all images is 1 × 1 μm^2.

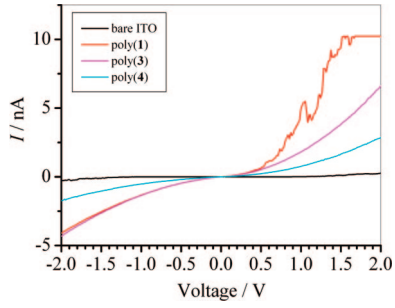

Figure 6. Current−voltage curves for the bare ITO and coated with electrochemically undoped 2,2′-carboranyldithiophene electropolymerized films, acquired under ambient conditions. All the measurements were performed with the same conducting AFM tip which was positively biased.

current conduction for the three polymer films, the peripheral regions surrounding the globular domains displayed higher conductivity than the surface areas of the protrusions.

To quantify the variation of the local conductance, current−voltage (*I-V*) plots were performed as a function of the applied voltage, which was linearly scanned between +2 and −2 V. Representative curves for the three electrochemically undoped polymer samples are shown in Figure 6. The thickness of the polymer samples (not determined) was believed to be similar because the same charge was consumed for their potentiodynamical electropolymerization (see the Experimental Section). Additionally, considering that the same contact force was applied to each sample, the differences in the current measured for each polymer can be confidently related to the differences in their conductivity properties. From curves in Figure 6, it is clear that the polymer conductivity decreased in the order poly(**1**) > poly(**3**) > poly(**4**), which is consistent with their electrochemical and optical characteristics. Control measurement at the bare ITO yielded the expected relatively less conductive behavior in the range of ±2.0 V. Furthermore, the *I*−*V* curve of poly(**1**) is slightly asymmetrical with respect to 0 V, whereas those for poly(**3**) and poly(**4**) are found to be more symmetrical. For example, the rectification factor measured at ±1.5 V decreased in the order poly(**1**) (4.0) > poly(**4**) (1.5) ∼ poly(**3**) (1.4). The weak or non asymmetry of the *I*−*V* curves suggests that the three carborane-functionalized polymers behave like heavily doped semiconductors rather than pure semiconductors for which much more asymmetrical current responses are usually observed.[57,58]

4. Concluding Remarks

As demonstrated in this study, the nature of the carborane isomer was found to strongly affect the electronic properties of the corresponding electrogenerated conducting polythiophene films. In particular, the introduction of *o*-carborane in the monomer pattern yielded a more conjugated and more conducting material compared with those electrogenerated from the *meta* and *para* isomers. As a matter of fact, the electrooxidation of the *ortho* isomer led to the deposition of a fused polythiophene backbone as a result of an electrochemical intramolecular cyclization of the two 2-thienyl rings. Such a hypothesis, consistent with the experimental results, was supported by theoretical calculations. Toward the challenging goal of designing heat-resistant conducting materials, the conductivity of these materials will be investigated as a function of temperature to evaluate the correlation with their previously reported high thermal stability.[31]

Acknowledgment. We thank the CINES (Centre Informatique National de l′Enseignement Supérieur, Montpellier) for computing time.

References and Notes

(1) Skotheim, T. A.; Reynolds, J. R. *Handbook of Conducting Polymers*, 3rd ed.; CRC Press, Taylor and Francis Group: Boca Raton, FL, 2007.
(2) Roncali, J. *Chem. Rev.* **1992**, *92*, 711.
(3) Thomas, S. W., III; Joly, G. D.; Swager, T. M. *Chem. Rev.* **2007**, *107*, 1339.
(4) Tourillon, G.; Garnier, F. *J. Electroanal. Chem.* **1982**, *135*, 173.
(5) Diaz, A. F.; Kanazawa, K. K.; Gardini, G. P. *J. Chem. Soc., Chem. Commun.* **1979**, 635.
(6) Andrieux, C. P.; Audebert, P.; Hapiot, P.; Savéant, J.-M. *J. Phys. Chem.* **1991**, *95*, 10158.
(7) Hatchett, D. W.; Josowicz, M. *Chem. Rev.* **2008**, *108*, 746.
(8) Lu, W.; Fadeev, A. G.; Qi, B.; Smela, E.; Mattes, B. R.; Ding, J.; Spinks, G. M.; Mazurkiewicz, J.; Zhou, D.; Wallace, G. G.; MacFarlane, D. R.; Forsyth, S. A.; Forsyth, M. *Science* **2002**, *297*, 983.
(9) Marinakos, S. M.; Shultz, D. A.; Feldheim, D. L. *Adv. Mat.* **1999**, *11*, 34.
(10) Leroux, Y.; Eang, E.; Fave, C.; Trippe, G.; Lacroix, J.-C. *Electrochem. Commun.* **2007**, *9*, 1258.
(11) Heeney, M.; Bailey, C.; Genevicius, K.; Shkunov, M.; Sparrowe, D.; Tierney, S.; McCulloch, I. *J. Am. Chem. Soc.* **2005**, *127*, 1078.
(12) Sivula, K.; Luscombe, C. K.; Thompson, B. C.; Fréchet, J. M. J. *J. Am. Chem. Soc.* **2006**, *128*, 13988.
(13) Pan, H.; Li, Y.; Wu, Y.; Liu, P.; Ong, B. S.; Zhu, S.; Xu, G. *J. Am. Chem. Soc.* **2007**, *129*, 4112.
(14) Zhao, C.-H.; Wakamiya, A.; Inukai, Y.; Yamagucgi, S. *J. Am. Chem. Soc.* **2006**, *128*, 15934.
(15) Simon, Y. C.; Ohm, C.; Zimny, M. J.; Coughlin, E. B. *Macromolecules* **2007**, *40*, 5628.
(16) Reed, C. A. *Acc. Chem. Res.* **1998**, *31*, 133.
(17) Plesek, J. *Chem. Rev* **1992**, *92*, 269, and references therein.
(18) Hawthorne, M. F.; Young, D. C.; Andrews, T. D.; Howe, D. V.; Pilling, R. L.; Pitts, A. D.; Reintjes, M.; Warren, L. F., Jr.; Wegner, P. A. *J. Am. Chem. Soc.* **1968**, *90*, 879.
(19) Hawthorne, M. F.; Young, D. C.; Wegner, P. A. *J. Am. Chem. Soc.* **1965**, *87*, 1818.
(20) Kabachii, Y. A.; Valetskii, P. M. *Int. J. Polym. Mater.* **1990**, *14*, 263.
(21) Schöberl, U.; Magnera, T. F.; Harrison, R. M.; Fleischer, F.; Pflug, J. L.; Schwab, P. F. H.; Meng, X.; Lipiak, D.; Noll, B. C.; Allured, V. S.; Rudalevige, T.; Lee, S.; Michl, J. *J. Am. Chem. Soc.* **1997**, *119*, 3907.
(22) Colquhoun, H. M.; Herbertson, P. L.; Wade, K.; Baxter, I.; Williams, D. J. *Macromolecules* **1998**, *31*, 1694.
(23) Fox, M. A.; Wade, K. *J. Mater. Chem.* **2002**, *12*, 1301.
(24) Kimura, H.; Okita, K.; Ichitani, M.; Sugimoto, T.; Kuroki, S.; Ando, I. *Chem. Mater.* **2003**, *15*, 355.
(25) Bekasova, N. I. *Russ. Chem. Rev.* **1984**, *53*, 61.
(26) David, V.; Vinas, C.; Teixidor, F. *Polymer* **2006**, *47*, 4694.
(27) Masalles, C.; Borros, S.; Vinas, C.; Teixidor, F. *Adv. Mater.* **2000**, *12*, 1199.
(28) Masalles, C.; Borros, S.; Vinas, C.; Teixidor, F. *Adv. Mater.* **2002**, *14*, 449.
(29) Masalles, C.; Llop, J.; Vinas, C.; Teixidor, F. *Adv. Mater.* **2002**, *14*, 826.
(30) Hao, E.; Fabre, B.; Fronczek, F. R.; Vicente, M. G. H. *Chem. Mater.* **2007**, *19*, 6195.
(31) Hao, E.; Fabre, B.; Fronczek, F. R.; Vicente, M. G. H. *Chem. Commun.* **2007**, 4387.
(32) Fabre, B.; Clark, J. C.; Vicente, M. G. H. *Macromolecules* **2006**, *39*, 112.
(33) Fabre, B.; Chayer, S.; Vicente, M. G. H. *Electrochem. Commun.* **2003**, *5*, 431.
(34) Zhan, X. W.; Yang, M. J.; Xu, G.; Liu, X. C.; Ye, P. X. *Macromol. Rapid Commun.* **2001**, *22*, 358.
(35) Hohenberg, P.; Kohn, W. *Phys. Rev.* **1964**, *136*, B864.
(36) Parr, R. G.; Yang, W. *Density-Functional Theory of Atoms and Molecules*; Oxford University Press: Oxford, U.K., 1989.
(37) Becke, A. D. *Phys. Rev.* **1988**, *38*, 3098.
(38) Becke, A. D. *J. Chem. Phys.* **1993**, *98*, 1372.
(39) Becke, A. D. *J. Chem. Phys.* **1993**, *98*, 5648.
(40) Lee, C.; Yang, W.; Parr, R. G. *Phys. Rev. B* **1988**, *37*, 785.
(41) Frisch, M. J.; Trucks, G. W.; Schlegel, H. B.; Scuseria, G. E.; Robb, M. A.; Cheeseman, J. R.; Montgomery, J., J. A.; Vreven, T.; Kudin, K. N.; Burant, J. C.; Millam, J. M.; Iyengar, S. S.; Tomasi, J.; Barone, V.; Mennucci, B.; Cossi, M.; Scalmani, G.; Rega, N.; Petersson, G. A.; Nakatsuji, H.; Hada, M.; Ehara, M.; Toyota, K.; Fukuda, R.; Hasegawa, J.; Ishida, M.; Nakajima, T.; Honda, Y.; Kitao, O.; Nakai, H.; Klene, M.; Li, X.; Knox, J. E.; Hratchian, H. P.; Cross, J. B.; Adamo, C.; Jaramillo, J.; Gomperts, R.; Stratmann, R. E.; Yazyev, O.; Austin, A. J.; Cammi, R.; Pomelli, C.; Ochterski, J. W.; Ayala, P. Y.; Morokuma, K.; Voth, G. A.; Salvador, P.; Dannenberg, J. J.; Zakrzewski, V. G.; Dapprich, S.; Daniels, A. D.; Strain, M. C.; Farkas, O.; Malick, D. K.; Rabuck, A. D.; Raghavachari, K.; Foresman, J. B.; Ortiz, J. V.; Cui, Q.; Baboul, A. G.; Clifford, S.; Cioslowski, J.; Stefanov, B. B.; Liu, G.; Liashenko, A.; Piskorz, P.; Komaromi, I.; Martin, R. L.; Fox, D. J.; Keith, T.; Al-Laham, M. A.; Peng, C. Y.; Nanayakkara, A.; Challacombe, M.; Gill, P. M. W.; Johnson, B.; Chen, W.; Wong, M. W.; Gonzalez, C.; Pople, J. A. *Gaussian 03, Revision D.02*; Gaussian, Inc.: Pittsburgh PA, 2003.
(42) Hariharan, P. C.; Pople, J. A. *Chem. Phys. Lett.* **1972**, *16*, 217.
(43) Flükiger, H. P.; Lüthi, S.; Portmann, S.; Weber, J. *MOLEKEL* version 4.3; Swiss National Supercomputing Centre CSCS: Manno, Switzerland, 2000.
(44) Zakharkin, L. I. *Pure Appl. Chem.* **1972**, *29*, 513.
(45) Schreber, R.; Grez, P.; Cury, P.; Veas, C.; Merino, M.; Gomez, H.; Cordova, R.; del Valle, M. A. *J. Electroanal. Chem.* **1997**, *430*, 77.
(46) Harrison, J. A.; Thirsk, H. R. The Fundamentals of Metal Deposition. in *Electroanalytical Chemistry, A Series of Advances*; Bard, A. J., Ed.; Vol. 5; Marcel Dekker, New York, 1971; p 89.
(47) Downard, A. J.; Pletcher, D. *J. Electroanal. Chem.* **1986**, *206*, 139.
(48) Hillman, A. R.; Mallen, E. F. *J. Electroanal. Chem.* **1987**, *220*, 351.
(49) Roncali, J. *Chem. Rev.* **1997**, *97*, 173.
(50) Reynolds, J. R.; Ruiz, J. P.; Child, A. D.; Nayak, K.; Marynick, D. S. *Macromolecules* **1991**, *24*, 678.
(51) Klein, D. L.; McEuen, P. L.; Bowen-Katari, J. E.; Alivisatos, A. P. *Nanotechnology* **1996**, *7*, 397.
(52) Klein, D. L.; McEuen, P. L. *Appl. Phys. Lett.* **1995**, *66*, 2478.
(53) Wold, D. J.; Frisbie, C. D. *J. Am. Chem. Soc.* **2000**, *122*, 2970.
(54) Rawlett, A. M.; Hopson, T. J.; Nagahar, L. A.; Tsui, R. K.; Ramachandran, G. K.; Lindsay, S. M. *Appl. Phys. Lett.* **2002**, *81*, 3043.
(55) Saitou, M.; Makabe, A.; Tomoyose, T. *Europhys. Lett.* **2000**, *52*, 185.
(56) Liau, Y.-H.; Scherer, N. F.; Rhodes, K. *J. Phys. Chem. B* **2001**, *105*, 3282.
(57) Lee, H. J.; Park, S.-M. *J. Phys. Chem. B* **2004**, *108*, 1590.
(58) Wu, C.-G.; Chang, S.-S. *J. Phys. Chem. B* **2005**, *109*, 825.
(59) Wilcox, D.; Dove, B.; McDavid, D.; Greer, D. *UTHSCSA Image Tool for Windows version 3.00*; The University of Texas Health Science Center: San Antonio, TX, 1995−2002.

MA802369Z